INTERNATIONAL JOURNAL FOR NUMERICAL METHODS IN FLUIDS
Int. J. Numer. Meth. Fluids 2003; **41**:275–301 (DOI: 10.1002/fld.432)

Equilibrium real gas computations using Marquina's scheme

Youssef Stiriba[†], Antonio Marquina[*,‡] and Rosa Donat[§]

Departament de Matemàtica Aplicada, 46100-Burjassot, Universitat de València, València, Spain

SUMMARY

Marquina's approximate Riemann solver for the compressible Euler equations for gas dynamics is generalized to an arbitrary equilibrium equation of state. Applications of this solver to some test problems in one and two space dimensions show the desired accuracy and robustness. Copyright © 2003 John Wiley & Sons, Ltd.

KEY WORDS: Riemann solver; compressible Euler equations; real gas

1. INTRODUCTION

Most modern shock capturing methods for compressible flow simulations are based on upwind differencing, and can be categorized into two general approaches: flux-difference splitting (FDS) and flux-vector splitting (FVS). The FDS uses either exact or approximate solutions of the local Riemann problem between adjacent states to get a set of waves and speeds, after field-by-field decomposition, and upwinding to distinguish between the influence of the moving waves across the cell interface for time marching. The FVS ignores the interaction between moving waves, and splits the flux vector of mass, momentum and energy into a left-going portion and a right-going portion to introduce an upwind bias.

While both the FVS and the FDS have proven robustness and accuracy for a wide range of problems, there are special situations where computational difficulties can arise in solving the Euler equations, such as the overheating phenomenon in wall-shock reflection problems (see References [1, 2]), the carbuncle phenomenon and others (see Reference [3]).

* Correspondence to: A. Marquina, Departament de Matemàtica Aplicada, Universitat de València, 46100-Burjassot, València, Spain.
† E-mail: stiriba@dpt.matapl.uv.es
‡ E-mail: marquina@uv.es
§ E-mail: donat@uv.es

Contract/grant number: PB97-1402

Received 25 April 2000
Revised 19 April 2002

Donat and Marquina [2] introduced a new upwind-biased FVS method for approximating solutions of hyperbolic systems of conservation laws. The basic scheme, a hybridization of the Steger-warming FVS (SW-FVS) and the local Lax-Friedrichs (LLF) for the ideal gas, corrects the lack of dissipation of the SW-FVS by introducing the more diffusive LLF in the neighbourhood of the sonic points. This produces numerical approximations in which the non-physical pathologies mentioned in Reference [3] are considerably reduced.

All of these approaches use the characteristic structure of the flux Jacobian matrix, and the algebraic simplicity of the polytropic ideal gas equation of state. However, the current interest in high-temperature gas, for which air cannot be considered thermally and calorically a perfect gas, has lead to various extensions of the FVS and FDS schemes to real gases, i.e. a gas in which intermolecular forces are taken into account. Various extensions of either FVS or FDS are considered in References [4–9] and we refer the interested reader to these papers for specific details.

The aim of this work is to analyse Marquina's FVS scheme for the Euler equations of compressible flow in equilibrium real gases. The behaviour of single-phase Navier–Stokes gases is determined by the so-called *fundamental derivative*, given by

$$\Gamma = \frac{1}{\rho}\frac{\partial(\rho c)}{\partial \rho}\bigg|_{s=\text{constant}} \tag{1}$$

where s is the entropy, ρ is the density, and $c = (\partial p/\partial \rho)|_s^{1/2}$ is the sound speed (p stands for pressure). We shall only consider real gases with $\Gamma > 0$, including some special van der Waals gases. When $\Gamma > 0$ for all ρ and s, all shocks are compression shocks, i.e. the pressure and density of the gas increases across the shock wave.

This work is organized as follows: in Section 2, we review the equations of flow for a general convex equation of state and the corresponding Jacobian flux matrix and its eigensystems, which form the ingredients needed in our code. Marquina's approach is briefly reviewed in Section 3. In Section 4 we give a constant entropy isobaric fix for both Stiffened and van der Waals equations of state. In Section 5 we display numerical results on test problems for shock reflection and shock tube problems in 1-D, and the problem of Mach 3 flow in a tunnel with a step in 2-D cartesian co-ordinates, for real gases governed by the above-mentioned equations of state. These tests validate Marquina's flux split formula for real gases and confirm that, as in the ideal gas case, this flux formula leads to a fairly robust and accurate numerical scheme in which certain pathological behaviour known to occur in numerical simulations with Godunov-type scheme is reduced to computationally acceptable levels.

2. THE FLOW EQUATIONS

2.1. 1-D Euler equations

The one-dimensional compressible Euler equations written conservation form

$$\frac{\partial \mathbf{q}}{\partial t} + \frac{\partial \mathbf{f}}{\partial x} = 0 \tag{2}$$

where $\mathbf{q}$ is the state vector of the conserved quantities and $\mathbf{f}$ is the flux function, are given by

$$\mathbf{q}=\begin{pmatrix}\rho\\ m\\ E\end{pmatrix},\quad \mathbf{f}(\mathbf{q})=\begin{pmatrix}m\\ \rho u^2+p\\ u(E+p)\end{pmatrix} \tag{3}$$

$$E=\rho e+\frac{\rho u^2}{2} \tag{4}$$

where ρ is the density, $m=\rho u$ is the momentum, E is the total energy per unit volume, u is the velocity, e is the internal energy per unit mass and p is the pressure related to these quantities via an equation of state (EOS), which is a relationship that describes the equilibrium thermodynamic properties of the fluid material, and it is assumed to be written as

$$p=p(\rho,e)=p(\tau,e) \tag{5}$$

where $\tau=\rho^{-1}$ is the specific volume. We will assume that

$$p_\tau<0 \quad \text{and} \quad p_e>0 \tag{6}$$

These conditions guarantee the hyperbolicity of system (3), (see Reference [5] and references therein).

For a polytropic ideal gas, Equation (5) is given by

$$p=(\gamma-1)\left(E-\frac{\rho u^2}{2}\right),\quad \gamma>1 \tag{7}$$

The ratio of heats γ takes the value $\frac{5}{3}$ for a mono-atomic gas and the value 1.4 for air.

In this section, we give simple analytical expressions for the spectral decomposition of the flux Jacobian matrix

$$\mathbf{A}(\mathbf{q})=\begin{pmatrix}0 & 1 & 0\\ c^2-u^2-\dfrac{p_e}{\rho}(H-u^2) & 2u-\dfrac{up_e}{\rho} & \dfrac{p_e}{\rho}\\ u(c^2-H)-\dfrac{up_e}{\rho}(H-u^2) & H-\dfrac{u^2p_e}{\rho} & u+\dfrac{up_e}{\rho}\end{pmatrix} \tag{8}$$

where c^2 is the sound speed

$$c^2=\frac{pp_e}{\rho^2}+p_\rho \tag{9}$$

H is the enthalpy

$$H=\frac{E+p}{\rho}=\frac{p}{\rho}+e+\frac{1}{2}u^2 \tag{10}$$

and

$$p_\rho=\frac{\partial p}{\partial \rho}(\rho,e),\quad p_e=\frac{\partial p}{\partial e}(\rho,e) \tag{11}$$

The eigenvalues of the Jacobian matrix are

$$\lambda_1(\mathbf{q}) = u - c, \quad \lambda_2(\mathbf{q}) = u, \quad \lambda_3(\mathbf{q}) = u + c \tag{12}$$

The corresponding right eigenvectors are given by

$$\mathbf{r}^1(\mathbf{q}) = \begin{pmatrix} 1 \\ u - c \\ H - uc \end{pmatrix}, \quad \mathbf{r}^2(\mathbf{q}) = \begin{pmatrix} 1 \\ u \\ H - \dfrac{\rho c^2}{p_e} \end{pmatrix}, \quad \mathbf{r}^3(\mathbf{q}) = \begin{pmatrix} 1 \\ u + c \\ H + uc \end{pmatrix} \tag{13}$$

The left eigenvectors $\{\mathbf{l}^k(\mathbf{q})\}_{k=1}^3$ are bi-orthonormal to $\{\mathbf{r}^k(\mathbf{q})\}_{k=1}^3$, i.e.

$$\mathbf{l}^i(\mathbf{q}) \cdot \mathbf{r}^j(\mathbf{q}) = \delta_{ij} \tag{14}$$

where δ_{ij} is the Kronecker symbol. To compute $\mathbf{l}^k(\mathbf{q})$ we first form the matrix of right eigenvectors

$$\mathbf{R}(\mathbf{q}) = (\mathbf{r}^1(\mathbf{q}), \mathbf{r}^2(\mathbf{q}), \mathbf{r}^3(\mathbf{q})) \tag{15}$$

Using (14), we get the matrix of left eigenvectors

$$\mathbf{L}(\mathbf{q}) = \mathbf{R}^{-1}(\mathbf{q}) \tag{16}$$

The row vector $\mathbf{l}^k(\mathbf{q})$, is defined to be the kth row in $\mathbf{L}(\mathbf{q})$. Then a complete set of left eigenvectors is

$$\mathbf{l}^1(\mathbf{q}) = \frac{1}{2}\begin{pmatrix} \dfrac{u}{c} + 1 - Y & -uX - \dfrac{1}{c} & X \end{pmatrix} \tag{17}$$

$$\mathbf{l}^2(\mathbf{q}) = \tfrac{1}{2}\begin{pmatrix} Y & uX - X \end{pmatrix} \tag{18}$$

$$\mathbf{l}^3(\mathbf{q}) = \frac{1}{2}\begin{pmatrix} 1 - \dfrac{u}{c} - Y & -uX + \dfrac{1}{c} & X \end{pmatrix} \tag{19}$$

where

$$X = \frac{p_e}{\rho c^2} \tag{20}$$

$$Y = (H - u^2)X \tag{21}$$

When the pressure is given by

$$p = (\gamma - 1)\rho e \tag{22}$$

one obtains expressions for the ideal gas case.

2.2. 2-D Euler equations

The two-dimensional compressible Euler equations are

$$\frac{\partial \mathbf{q}}{\partial t} + \frac{\partial \mathbf{f}}{\partial x} + \frac{\partial \mathbf{g}}{\partial y} = 0 \tag{23}$$

where

$$\mathbf{q} = \begin{pmatrix} \rho \\ \rho u \\ \rho v \\ E \end{pmatrix}, \quad \mathbf{f}(\mathbf{q}) = \begin{pmatrix} \rho u \\ \rho u^2 + p \\ \rho uv \\ (E+p)u \end{pmatrix}, \quad \mathbf{g}(\mathbf{q}) = \begin{pmatrix} \rho v \\ \rho uv \\ \rho v^2 + p \\ (E+p)v \end{pmatrix} \tag{24}$$

$$E = \rho e + \frac{\rho(u^2+v^2)}{2} \tag{25}$$

where u and v are the velocities in the x- and y-directions, respectively, and $p = p(\rho, e)$.

As in the 1-D Euler equations, we give analytical expressions for the spectral decomposition of the Jacobian matrices $\mathbf{A}(\mathbf{q}) = \partial \mathbf{f}/\partial \mathbf{q}$ and $\mathbf{B}(\mathbf{q}) = \partial \mathbf{g}/\partial \mathbf{q}$ in terms of the thermodynamic derivatives obtained from the (EOS).

The Jacobian matrix of the flux $\mathbf{f}(\mathbf{q})$ is

$$\mathbf{A}(\mathbf{q}) = \begin{pmatrix} 0 & 1 & 0 & 0 \\ c^2 - X^2 - \dfrac{p_e}{\rho}(H - q^2) & 2X - \dfrac{Xp_e}{\rho} & -\dfrac{Yp_e}{\rho} & \dfrac{p_e}{\rho} \\ -uv & Y & X & 0 \\ X(c^2 - H) - \dfrac{Xp_e}{\rho}(H - q^2) & H - \dfrac{X^2 p_e}{\rho} & -\dfrac{uvp_e}{\rho} & X + \dfrac{Xp_e}{\rho} \end{pmatrix} \tag{26}$$

The eigenvalues are

$$\lambda_1(\mathbf{q}) = X - c, \quad \lambda_2(\mathbf{q}) = \lambda_3(\mathbf{q}) = X, \quad \lambda_4(\mathbf{q}) = X + c \tag{27}$$

A complete set of right eigenvectors is

$$\mathbf{r}^1(\mathbf{q}) = \begin{pmatrix} 1 \\ X - c \\ Y \\ H - Xc \end{pmatrix}, \quad \mathbf{r}^2(\mathbf{q}) = \begin{pmatrix} 0 \\ 0 \\ 1 \\ Y \end{pmatrix} \tag{28}$$

$$\mathbf{r}^3(\mathbf{q}) = \begin{pmatrix} 1 \\ X \\ Y \\ H - \dfrac{\rho c^2}{p_e} \end{pmatrix}, \quad \mathbf{r}^4(\mathbf{q}) = \begin{pmatrix} 1 \\ X + c \\ Y \\ H + Xc \end{pmatrix} \tag{29}$$

The corresponding right and left eigenvectors are

$$\mathbf{l}^1(\mathbf{q}) = \begin{pmatrix} \frac{b_2}{2} + \frac{X}{2c} & -\frac{b_1 X}{2} - \frac{1}{2c} & -\frac{b_1 Y}{2} & \frac{b_1}{2} \end{pmatrix} \tag{30}$$

$$\mathbf{l}^2(\mathbf{q}) = \begin{pmatrix} -Y & 0 & 1 & 0 \end{pmatrix} \tag{31}$$

$$\mathbf{l}^3(\mathbf{q}) = \begin{pmatrix} 1 - b_2 & b_1 X & b_1 Y & -b_1 \end{pmatrix} \tag{32}$$

$$\mathbf{l}^4(\mathbf{q}) = \begin{pmatrix} \frac{b_2}{2} - \frac{X}{2c} & -\frac{b_1 X}{2} + \frac{1}{2} & -\frac{b_1 Y}{2} & \frac{b_1}{2} \end{pmatrix} \tag{33}$$

where

$$q^2 = u^2 + v^2, \quad c^2 = p_\rho + \frac{p p_e}{\rho^2} \tag{34}$$

$$H = \frac{E + p}{\rho}, \quad X = u, \quad Y = v \tag{35}$$

$$b_1 = \frac{p_e}{\rho c^2}, \quad b_2 = 1 + (q^2 - H) b_1 \tag{36}$$

The Jacobian matrix of the flux function $\mathbf{g}(\mathbf{q})$ and its eigensystem are obtained from those of $\mathbf{f}(\mathbf{q})$ by interchanging the second and third rows, and columns, and setting $X = v$ and $Y = u$.

2.3. *Equations of state*

We consider here two equations of state which we will use in the numerical computations, written in the general form

$$p = p(\rho, e) \tag{37}$$

Stiffened gas EOS: The Stiffened gas EOS is a reasonable approximation for gases, liquids, and solids under high-pressure conditions. Such equation is obtained by linearization near a reference state from a Gruneisen equation of state for metal [10]

$$p = (\gamma - 1)\rho e + C\left(\frac{\rho}{\rho_{\text{ref}}} - 1\right) \tag{38}$$

where ρ_{ref} is a reference density, and C is a constant depending on the gas. The thermodynamic derivatives used in our scheme are

$$p_\rho = (\gamma - 1)e + \frac{C}{\rho_{\text{ref}}} \quad \text{and} \quad p_e = (\gamma - 1)e \tag{39}$$

van der Waals EOS: This is an equation of state that takes into account the effects of attractive forces between the molecules [11], and it has the form

$$p(\rho, T) = \frac{RT}{\tau - b} - \frac{a}{\tau^2} \tag{40}$$

where T is the temperature, and the quantities a and b are the van der Waals gas constants that measure the molecule cohesive forces and the finite size of molecules, respectively

($a \geqslant 0, 0 \leqslant b < 1/\gamma$, see Reference [11] for numerical values to various gaseous substances). Since $e = e(\rho, T)$ and

$$\mathrm{d}e = \left(\frac{p - Tp_T}{\rho^2} \right) \mathrm{d}\rho + c_v \, \mathrm{d}T \tag{41}$$

Equation (40) may be written as

$$p(\rho, e) = \frac{\rho R}{1 - \rho b} \left(\frac{e + a\rho}{c_v} \right) - a\rho^2 \tag{42}$$

with

$$p_\rho = \frac{R}{c_v} \left(\frac{e + a\rho}{(1 - \rho b)^2} + \frac{\rho a}{1 - \rho b} \right) - 2a\rho \quad \text{and} \quad p_e = \frac{\rho R}{c_v (1 - \rho b)} \tag{43}$$

Here R is the specific gas constant, and c_v the specific heat at constant volume.

Note that a van der Waals gas (42) reduces to a Noble-Abel gas when $a = 0$. Polytropic gases are obtained for $b = 0$ as well.

3. MARQUINA'S METHOD FOR REAL GASES

Marquina's flux function, introduced by Donat and Marquina [2], is an extension of the upwind entropy fix of Shu and Osher [12] to systems of hyperbolic conservation laws within each cell. The Jacobian matrix $\mathbf{A}(\mathbf{q})$ at $\mathbf{q}$ is decomposed into its eigenvalues $\{\lambda_p(\mathbf{q})\}_{p=1}^m$, normalized right eigenvectors $\{\mathbf{r}^p(\mathbf{q})\}_{p=1}^m$ and normalized left eigenvectors $\{\mathbf{l}^p(\mathbf{q})\}_{p=1}^m$. These ingredients allow the application of Marquina's approach to the Euler equations for real gases in the one-dimensional case. Next, we briefly review the method and comment on specific issues related to the EOS for non-perfect gases.

Consider a cell wall, $x_{i+1/2}$, where we have to evaluate the numerical flux function $\mathbf{F}_{i+1/2}^n$, at a given time step n. We decompose the left state $\mathbf{Q}_i$, the right state $\mathbf{Q}_{i+1}$, and the flux function evaluated at these states into characteristic variables

$$\omega_i^p = \mathbf{l}^p(\mathbf{Q}_i).\mathbf{Q}_i, \quad \omega_{i+1}^p = \mathbf{l}^p(\mathbf{Q}_{i+1}).\mathbf{Q}_{i+1}$$

$$\phi_i^p = \mathbf{l}^p(\mathbf{Q}_i).\mathbf{f}(\mathbf{Q}_i), \quad \phi_{i+1}^p = \mathbf{l}^p(\mathbf{Q}_{i+1}).\mathbf{f}(\mathbf{Q}_{i+1})$$

for $p = 1, \ldots, m$. The characteristic numerical fluxes are

$$\phi_+^k = \phi_i^k \beta_k^+ \delta_k^+ - \tfrac{1}{2}(\phi_i^k + \alpha_k \omega_i^k)\beta_k^-$$

$$\phi_-^k = -\phi_{i+1}^k \beta_k^+ \delta_k^- - \tfrac{1}{2}(\phi_{i+1}^k - \alpha_k \omega_{i+1}^k)\beta_k^-$$

where

$$\beta_k = \mathrm{sign}(\lambda_k(\mathbf{Q}_i)) \, \mathrm{sign}(\lambda_k(\mathbf{Q}_{i+1}))$$

$$\delta_k = \mathrm{sign}(\lambda_k(\mathbf{Q}_i))$$

and

$$\alpha_k = \max_{\mathbf{q}\in\gamma_i(\mathbf{Q}_i,\mathbf{Q}_{i+1})} |\lambda_k(\mathbf{q})|$$

Here $\gamma_i(\mathbf{Q}_i, \mathbf{Q}_{i+1})$ is a curve in phase-space connecting $\mathbf{Q}_i$ and $\mathbf{Q}_{i+1}$. For the Euler equations of gas dynamics, the pth characteristic fields are genuinely non-linear or linearly degenerate (also in our real gas case since $\Gamma > 0$). In that case

$$\alpha_k = \max(|\lambda_k(\mathbf{Q}_i)|, |\lambda_k(\mathbf{Q}_{i+1})|)$$

Marquina's flux function is then

$$\mathbf{F}^{\mathrm{M}}(\mathbf{Q}_i, \mathbf{Q}_{i+1}) = \mathbf{F}^+ + \mathbf{F}^- \tag{44}$$

where

$$\mathbf{F}^+ = \sum_{p=1}^{m} \phi_+^p \mathbf{r}^p(\mathbf{Q}_i), \qquad \mathbf{F}^- = \sum_{p=1}^{m} \phi_-^p \mathbf{r}^p(\mathbf{Q}_{i+1}) \tag{45}$$

Marquina's scheme is consistent, i.e.

$$\mathbf{F}^{\mathrm{M}}(\mathbf{q}, \mathbf{q}) = \mathbf{f}(\mathbf{q}) \tag{46}$$

If all signal speeds $\lambda^p(\mathbf{Q}_i)$ and $\lambda^p(\mathbf{Q}_{i+1})$ are positive, then

$$\mathbf{F}^{\mathrm{M}}(\mathbf{Q}_i, \mathbf{Q}_{i+1}) = \mathbf{f}(\mathbf{Q}_i) \tag{47}$$

and when all signal speeds are negative

$$\mathbf{F}^{\mathrm{M}}(\mathbf{Q}_i, \mathbf{Q}_{i+1}) = \mathbf{f}(\mathbf{Q}_{i+1}) \tag{48}$$

When an eigenvalue changes sign, Marquina's flux function characteristic component is constructed from the local-Lax-Friedrichs scalar numerical flux, which introduces additional dissipation to enforce an entropy condition in the case of a rarefaction wave (when $\lambda^p(\mathbf{Q}_i) < 0 < \lambda^p(\mathbf{Q}_{i+1})$), or in other circumstances such as shock reflection (see References [2, 13]). The flux splitting and the Jacobian evaluation in the first-order scheme are based on the physical data on the left and right sides of the cell wall.

Marquina's scheme is thus a characteristic-based upwind scheme that, in contrast to the other upwind schemes, is free from either exact or approximate Riemann solvers in the case of non-linear systems.

The first-order scheme based on Marquina's flux function has conservation form

$$\mathbf{Q}_i^{n+1} = \mathbf{Q}_i^n - \frac{\Delta t}{\Delta x}(\mathbf{F}_{i+1/2}^n - \mathbf{F}_{i-1/2}^n)$$

with

$$\mathbf{F}_{i+1/2}^n = \mathbf{F}^{\mathrm{M}}(\mathbf{Q}_i, \mathbf{Q}_{i+1})$$

Higher accuracy can be achieved by evaluating the Jacobian matrices $\mathbf{A}(\mathbf{q}_{\mathrm{L}})$ and $\mathbf{A}(\mathbf{q}_{\mathrm{R}})$ at the left-side-biased interpolation of the conservative state $\mathbf{Q}_i$ and the right-side-biased interpolation of the conservative state $\mathbf{Q}_{i+1}$, respectively. Then, we use the eigenstructure of

the Jacobian matrices $\mathbf{A}(\mathbf{q}_L)$ and $\mathbf{A}(\mathbf{q}_R)$ separately to compute the numerical characteristic fluxes, by applying a non-linear high-order interpolation procedure on both the characteristic variables and characteristic fluxes ϕ^p and ω^p in space, leaving the problem continuous in time, and using the total variation diminishing Shu–Osher Runge–Kutta methods for the time evolution.

The states $\mathbf{q}_L$ and $\mathbf{q}_R$ on both sides of cell wall are interpolated using the same procedure as for the numerical characteristic fluxes. In our numerical experiments, the reconstruction step is performed on the conservative variables using the second-order ENO [12] and the third-order PHM [14] procedures together with the second- and third-order Runge–Kutta methods, respectively.

For multidimensional systems, we extend Marquina's scheme by the standard dimension by dimension technique, so that the 1-D algorithm applies in each spatial dimension.

Remark 1

For a polytropic ideal gas or a thermally (not necessarily calorically) perfect gas with EOS

$$p = \rho RT(e)$$

we have

$$p(\alpha\rho, e) = \alpha\, p(\rho, e)$$

Then, the physical flux is homogenous of degree 1, and Marquina's scheme is a non-linear hybridization of Steger and Warming FVS and LLF in each characteristic field. For an arbitrary equilibrium gas, the physical flux no longer possesses the homogeneity property and we cannot find a natural real-gas extension of Steger and Warming FVS, see Reference [9].

Remark 2

We note that for general EOS, the construction of some Riemann solvers is not unique and it is somewhat difficult [6, 9]. For example, for Roe FDS, a Roe matrix is not uniquely determined and numerical codes using such matrix need mean values of the thermodynamical derivatives p_ρ and p_e. Such quantities cannot be evaluated by their exact derivatives at mean values $\bar{\rho}$ and $\bar{e}$ without violating the condition

$$\Delta p = \bar{p}_e \Delta e + \bar{p}_\rho \Delta\rho$$

(see References [4, 6, 7, 9] for details). In Marquina's flux formula we use directly the point values of such derivatives, which may be computed easily from the EOS without using additional assumptions or approximations.

4. CONSTANT ENTROPY ISOBARIC FIX FOR STIFFENED AND VAN DER WAALS EOS

The constant entropy isobaric fix, recently derived by Fedkiw *et al.* [15], is a new method to fix the overheating errors which may occur when a shock reflects off a stationary solid wall boundary or near a material interface. The isobaric fix is applied as a boundary condition near the wall or interface by fixing pressure and velocity and enforcing constant entropy to get a

new density or temperature so that the total variation from the physical values is minimum (see Reference [15] for more details).

Fedkiw *et al.* [15] have written such entropy correction for ideal gases, tait solid, and virial EOS, and have pointed out the difficulty to apply it to other EOS. In this section, we give a constant entropy isobaric fix for both stiffened and van der Waals EOS.

Let us denote by 'a' the reference cell and by 'b' the cells to be corrected. The equation that guarantees constant entropy [15] is

$$\frac{\mathrm{d}e}{\mathrm{d}\rho} = \frac{p}{\rho^2} \tag{49}$$

We solve the initial value problem defined by this equation together with $\rho = \rho_a$ to get the corrected density ρ_b for the Stiffened gas EOS and the van der Waals EOS cases.

4.1. Stiffened EOS

Using the equation of state, Equation (49) can be rewritten as an initial value problem with a linear first-order ordinary differential equation

$$\frac{\mathrm{d}e}{\mathrm{d}\rho} = \frac{f(\rho)}{\rho^2} + \frac{g(\rho)}{\rho^2}\, e \tag{50}$$

where

$$f(\rho) = (\gamma - 1)\rho e \quad \text{and} \quad g(\rho) = C\left(1 - \frac{\rho}{\rho_{\mathrm{ref}}}\right) \tag{51}$$

We use the integrating factor $\mu = \rho^{1-\rho}$, and we get the following solution:

$$e = -\frac{C}{\gamma\rho} - \frac{C}{(\gamma - 1)\rho_{\mathrm{ref}}} + C(S)\rho^{\gamma - 1} \tag{52}$$

where $C(S)$ is a constant depending on the entropy S. We use the EOS to get

$$C(S) = \frac{p - C}{(\gamma - 1)\rho^{\gamma}} \tag{53}$$

or, equivalently

$$C'(S) = \frac{p - C}{\rho^{\gamma}} \tag{54}$$

Thus, the new density is

$$\rho_{\mathrm{new}} = \rho_a \left(\frac{p_b - C}{p_a - C}\right)^{1/\gamma} \tag{55}$$

4.2. van der Waals EOS

Using the equation of state, Equation (49) becomes

$$\frac{\mathrm{d}e}{\mathrm{d}\rho} = \frac{R}{c_v(1 - \rho b)\rho}\, e + \frac{aR}{c_v(1 - \rho b)} - a \tag{56}$$

integrating this ODE, we get the solution

$$e = C(S)\left(\frac{\rho}{1-\rho b}\right)^{R/c_v} - a\rho \tag{57}$$

We apply the EOS to obtain

$$C(S) = \frac{c_v}{R}(p + a\rho^2)\left(\frac{\rho}{1-\rho b}\right)^{-R/c_v - 1} \tag{58}$$

One can use the Newton–Raphson iteration

$$x_{n+1} = x_n - \frac{h(x_n)}{h'(x_n)} \tag{59}$$

$$x_0 = \rho_a \tag{60}$$

where

$$h(x) = \frac{c_v}{R}\left(\frac{x}{1-xb}\right)^{R/c_v + 1} - ax^2 - p_b \tag{61}$$

to approximate the new density ρ_{new}.

5. NUMERICAL EXPERIMENTS

We will use the first-, second-, and third-order TVD Runge–Kutta methods for time stepping, and the second-order ENO and the third-order PHM method for the spatial discretization. For the Stiffened gas EOS we consider $\gamma = 1.4$, and $C = 1$. For the van der Waals EOS we use $\gamma = 1.39$, $R = 0.0821\,\text{dm}^3\,\text{atm}\,\text{K}^{-1}\,\text{mol}^{-1}$, $a = 0.03412\,\text{dm}^6\,\text{atm}\,\text{mol}^{-2}$, $b = 0.23\,\text{dm}^3\,\text{mol}^{-1}$, and $c_v = 20.81\,\text{J}\,\text{K}^{-1}\,\text{mol}^{-1}$.

5.1. Shock-tube problem

The first test to validate the accuracy and robustness of the present flux split method is the shock tube problem. The initial data consists of two constants states separated by a diaphragm at $x = 0.5$. The left and the right states are given by

$$(\rho_{\text{L}}, u_{\text{L}}, p_{\text{L}}) = (1, 0, 1) \tag{62}$$

$$(\rho_{\text{R}}, u_{\text{R}}, p_{\text{R}}) = (0.125, 0, 0.1) \tag{63}$$

The solution contains four states separated by a shock wave, a contact surface, and an expansion wave. The numerical results, represented by circles, together with the exact solution represented by solid lines, are shown in Figures 1–4. One can see that the three waves are well resolved and that the present solver equipped with the ENO-2 and PHM-3

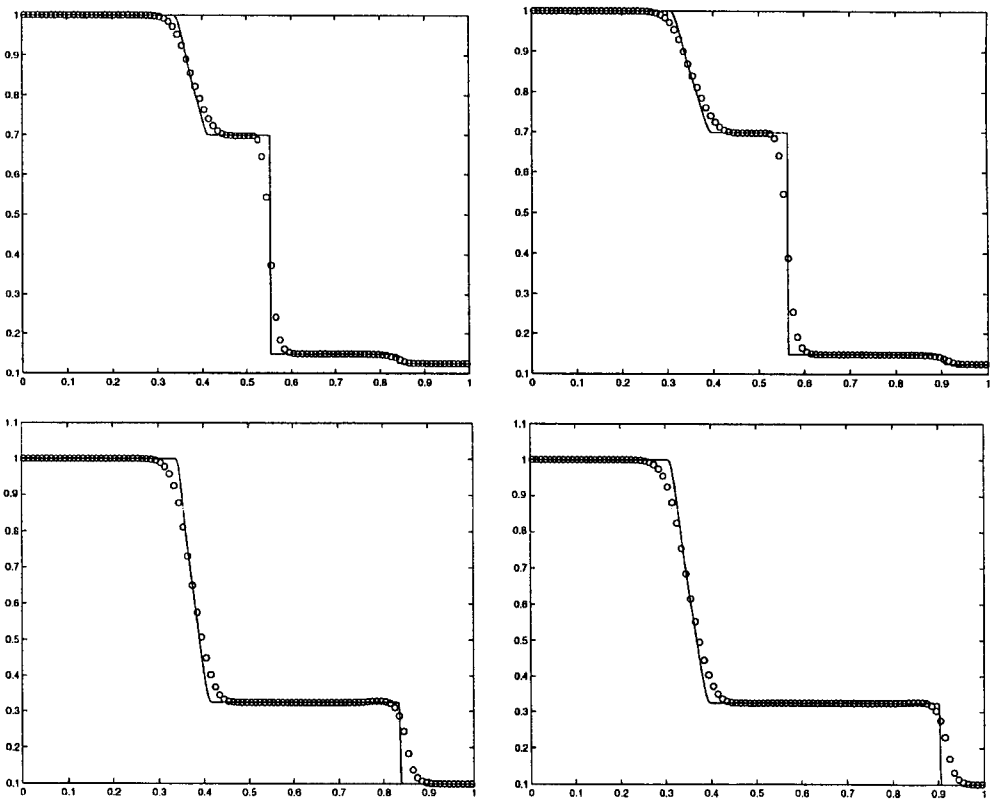

Figure 1. Stiffened EOS. Shock tube problem with ENO-2 scheme: density top, pressure left, at $t = 0.06$ left, $t = 0.09$ right. All the variables were computed on a equidistant grid of 100 zones.

reconstruction procedures converges to the entropy solution with good resolution. The numerical approximations agree well with the exact solution for both Stiffened and van der Waals EOS. Also, there are no noticeable pathologies or unwanted oscillations associated with any of them.

In the first two figures, which correspond to Stiffened EOS, the jump across the contact discontinuity is large if we compare it with the ideal gas case, but the numerical dissipation remains the same (usually 4 or 5 points in the surface position). A weaker shock wave is also observed. The scheme gives the correct shock position with a monotone profile and good resolution.

For van der Waals EOS, Figures 3 and 4, it appears that the scheme behaves as in the ideal gas case.

The results show that the third-order hyperbolic extension of the present scheme performs well and gives the best resolution.

In Figure 5 we have plotted the density obtained by the same procedures with the extension of van Leer flux vector splitting scheme [9] instead of the present solver. As we can see the results are nearly the same for both Stiffened and van der Waals EOS.

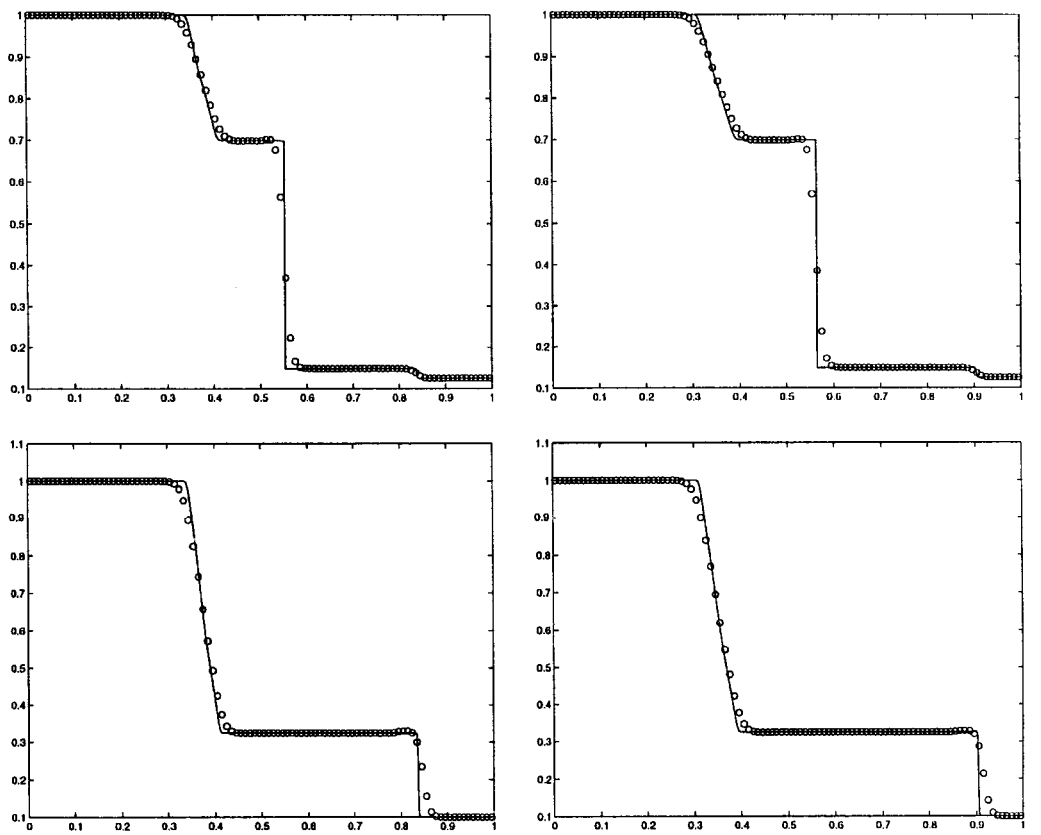

Figure 2. Stiffened EOS. Shock tube problem with PHM scheme: density top, pressure left, at $t = 0.06$ left, $t = 0.09$ right. All the variables were computed on a equidistant grid of 100 zones.

5.2. *Shock-reflection problem*

In this example we consider the problem of a strong shock reflection from a rigid wall in one dimension for real gases. The initial conditions consist of a gas of constant density and pressure moving towards $x = 0$ in the computational domain $[0, 1]$, i.e.

$$(p(x), u(x), e(x)) = (1, -1, 4), \quad 0 < x < 1 \tag{64}$$

The boundary at $x = 0$ is a solid wall.

The 'overheating effect' occurs in the first few zones near the wall, when the shock reflects off the stationary solid wall at the boundary. The overheating in the specific internal energy profile (peak) and the corresponding dip in the density are conspicuous, while the pressure and velocity have correct values.

Following Noh [1], this error is inevitable for any shock capturing method unsuccessful to model the heat conduction present in real fluids. He showed that a numerical scheme with a builtin heat conduction mechanism will be able to dissipate the overheating, i.e. the solution converges in the L^∞ sense.

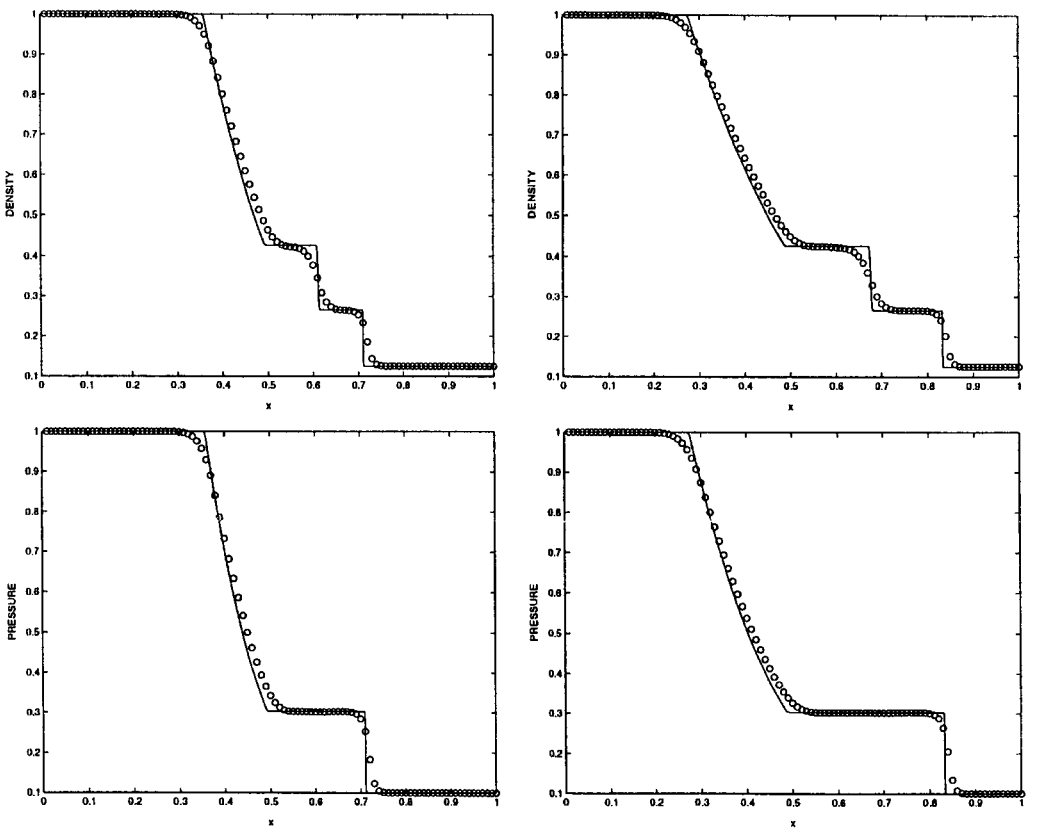

Figure 3. van der Waals EOS. Shock tube problem with ENO-2 scheme: density top, pressure left, at $t = 0.06$ left, $t = 0.09$ right. All the variables were computed on a equidistant grid of 100 zones.

Glaister [6, 7] has also observed the overheating error for other equations of state.

Figures 6 and 13 display numerical approximations obtained by the first-order scheme for both Stiffened and van der Waals EOS. Although we observe an overheating in density (whose value is around 1.5%) and the consequent dip in internal energy (of value less than 2%), this behaviour is by no means as extreme as the one observed in other real-gas experiments, e.g. Reference [6]. These plots show that the present flux-split method dissipates the overheating error to a numerically acceptable level also in the real-gas case.

The overheating error for real gases persists in time, but its magnitude decreases with time. The difference of the relative errors for Stiffened EOS. is less than 0.000341, and less than 0.000185 for van der Waals EOS, between $t = 1.5$ and 2, with $\Delta t/\Delta x = 0.1$ and 100 equally spaced points.

Our numerical experiments shown that the present scheme produces many intermediate states in the numerical shock layer. This is due to the fact that in such a region, near the reflecting boundary, the wavespeeds change sign, thus, our flux-split method adds dissipation. To reduce such dissipation, and to improve the overall resolution, we have experimented with a second and a third-order extension of the present scheme by ENO2 and PHM3 reconstructions,

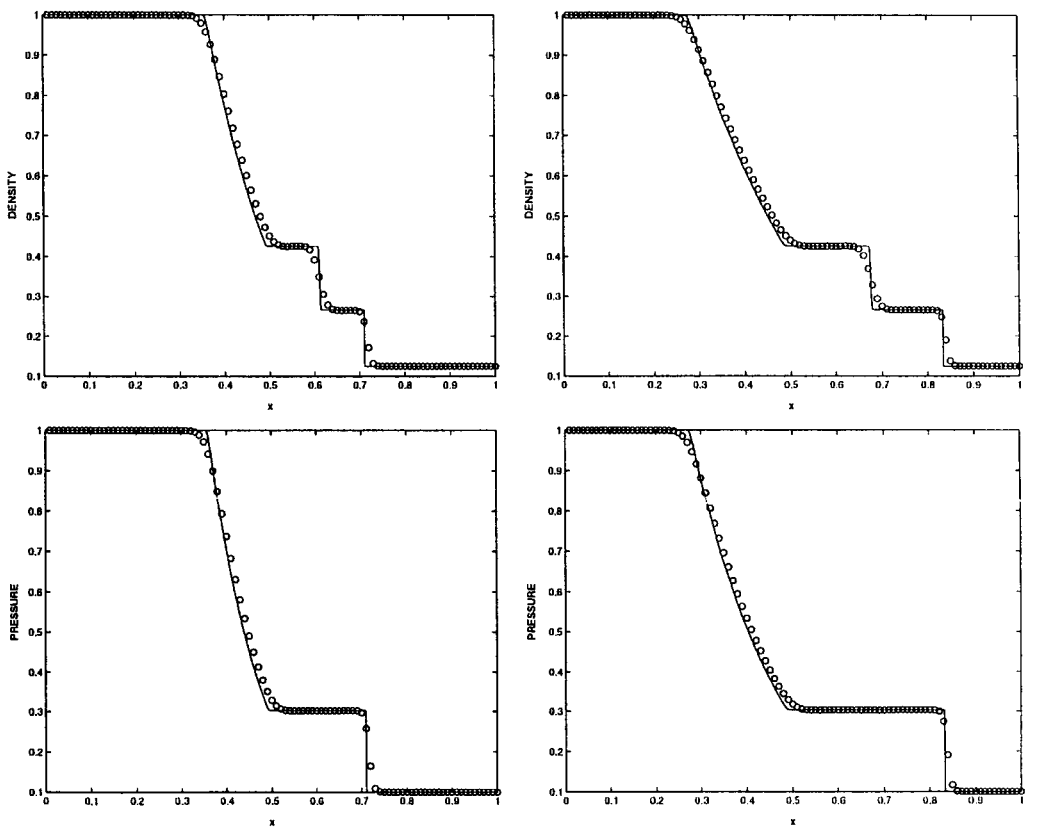

Figure 4. van der Waals EOS. Shock tube problem with PHM scheme: density top, pressure left, at $t = 0.06$ left, $t = 0.09$ right. All the variables were computed on a equidistant grid of 100 zones.

respectively. In Figures 7, 8,14 and 15, we display the density and internal energy (Figures 9–11). The results are consistent with those of the first-order scheme, in that we see an ordering of schemes (see also the closer look at the wall in the right side of Figures 12 and 19) first order, ENO-2, and PHM, in order of decreasing magnitude of error. Notice that the local hyperbolic reconstruction gives the best approximation near the wall and in the shock transition layer (Figures 13–19). For the sake of comparison, the left sides of Figures 12 and 19 show the numerical value obtained with van Leer scheme near the wall. The overheating is much visible in the first- and the third-order schemes near the wall. The second-order scheme gives similar results for Stiffened EOS as those obtained of our ENO2 method. Notice that the present solver combined with the local hyperbolic reconstruction gives the best approximation near the wall and in the shock transition layer.

5.3. A two-dimensional test

In this section, we consider the standard two-dimensional Mach 3 step flow test problem. This test has been used by Colella and Woodward [16] to compare the performance of various numerical schemes in ideal gas simulations.

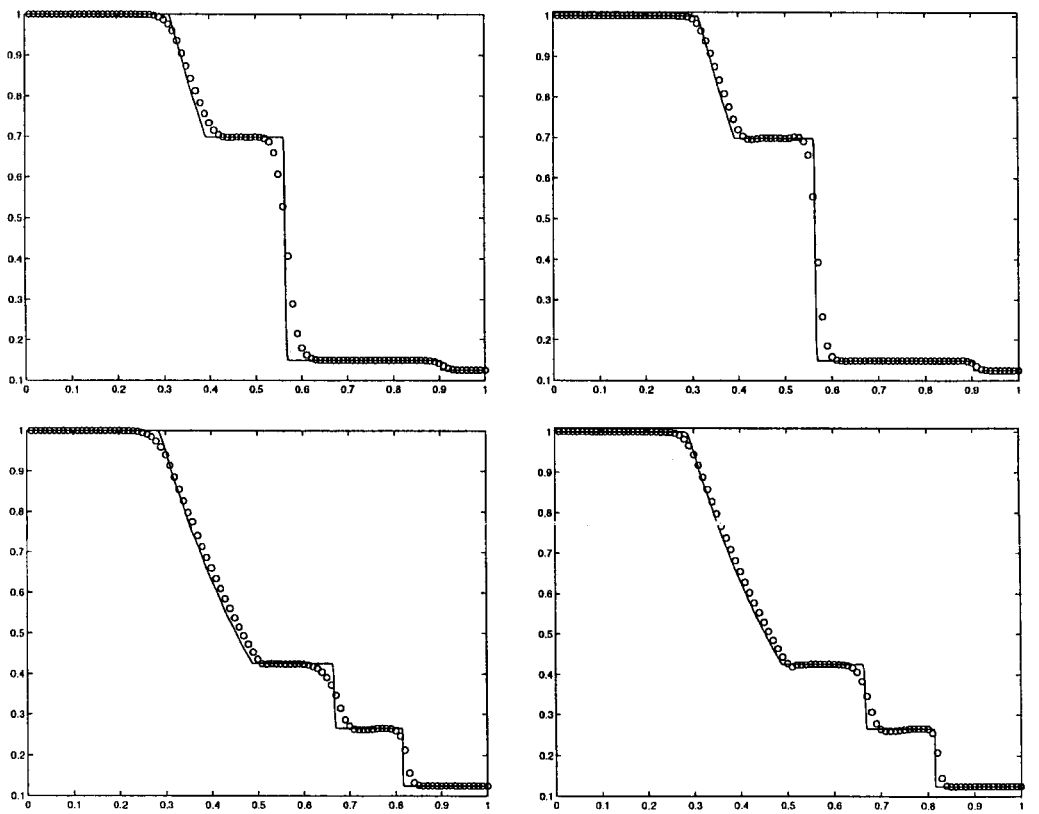

Figure 5. Shock tube problem with van Leer scheme, density, left: second-order scheme, right: third-order scheme right, top: Stiffened EOS top, and bottom: van der Waals EOS bottom.

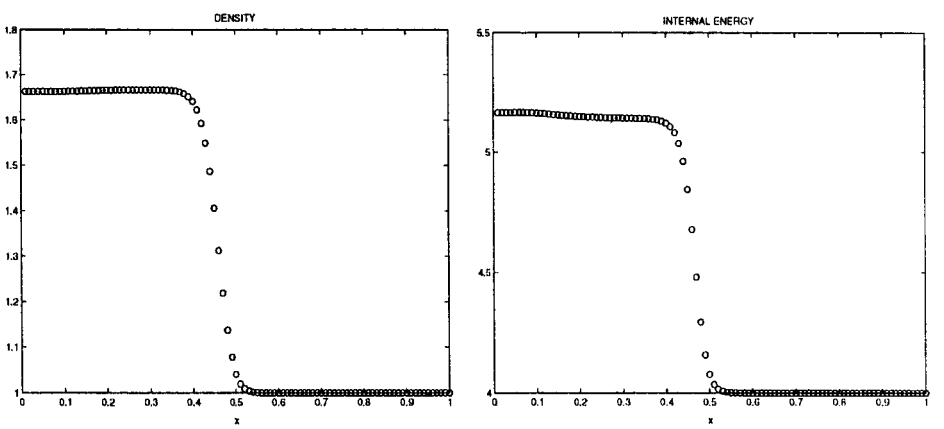

Figure 6. Stiffened EOS. Shock reflection problem with first-order scheme for time $t = 0.3$: density left, internal energy right. All the variables were computed on a equidistant grid of 100 zones.

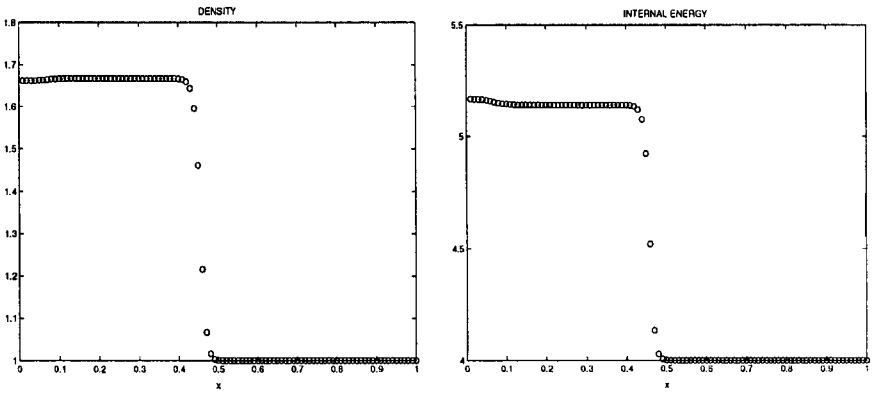

Figure 7. Stiffened EOS. Shock reflection problem with ENO-2 scheme for time $t = 0.3$: density left, internal energy right. All the variables were computed on a equidistant grid of 100 zones.

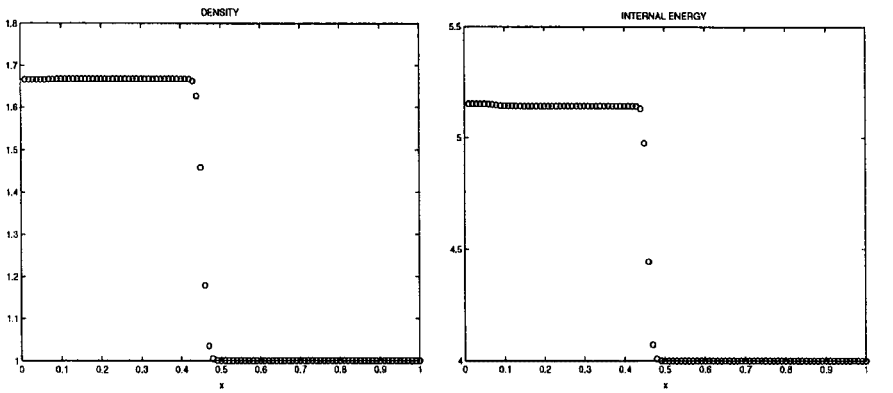

Figure 8. Stiffened EOS. Shock reflection problem with PHM scheme for time $t = 0.3$: density left, internal energy right. All the variables were computed on a equidistant grid of 100 zones.

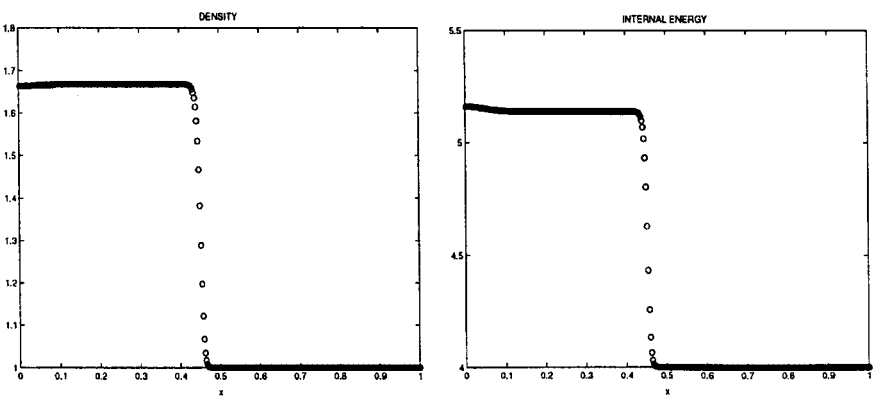

Figure 9. Stiffened EOS. Shock reflection problem with first-order scheme for time $t = 0.3$: density left, internal energy right. All the variables were computed on a equidistant grid of 400 zones.

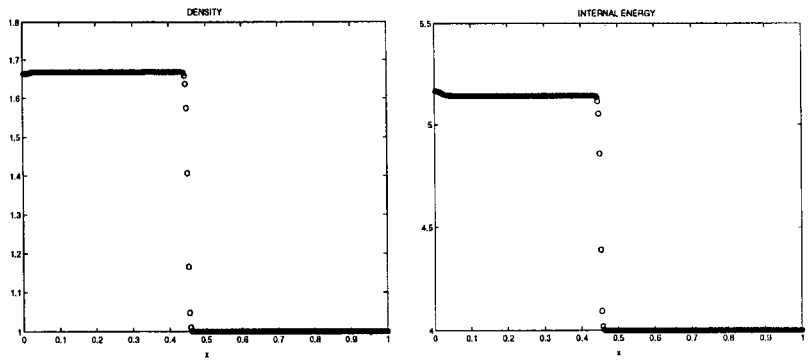

Figure 10. Stiffened EOS. Shock reflection problem with ENO-2 scheme for time $t = 0.3$: density left, internal energy right. All the variables were computed on a equidistant grid of 400 zones.

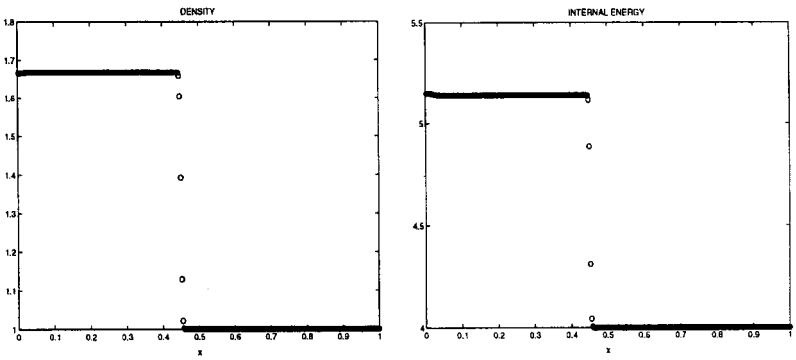

Figure 11. Stiffened EOS. Shock reflection problem with PHM scheme for time $t = 0.3$: density left, internal energy right. All the variables were computed on a equidistant grid of 400 zones.

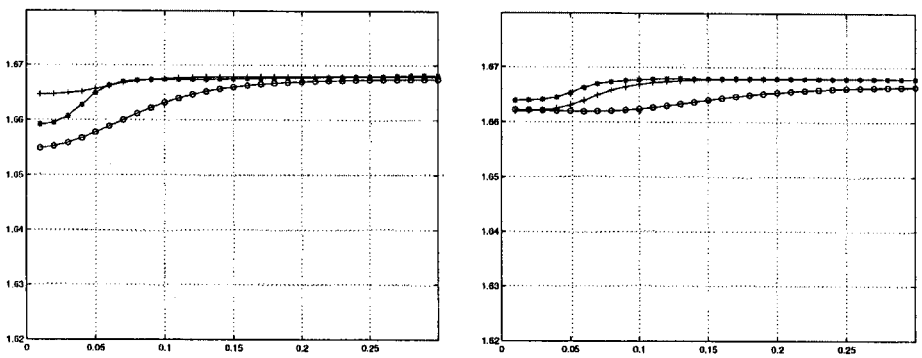

Figure 12. Stiffened EOS, a zoom of 30 grid zone next to the left wall on a 100 zones. Right: present scheme, left: van Leer scheme. o: first-order, +: ENO-2, and *: PHM.

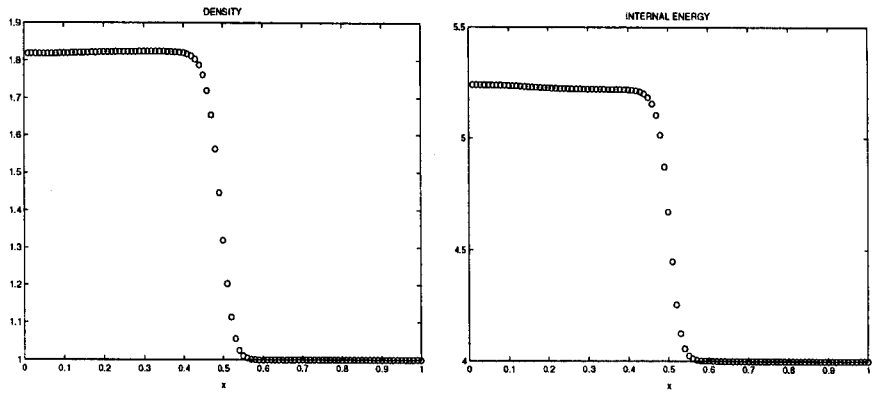

Figure 13. van der Waals EOS. Shock reflection problem with first-order scheme for time $t = 0.4$: density left, internal energy right. All the variables were computed on a equidistant grid of 100 zones.

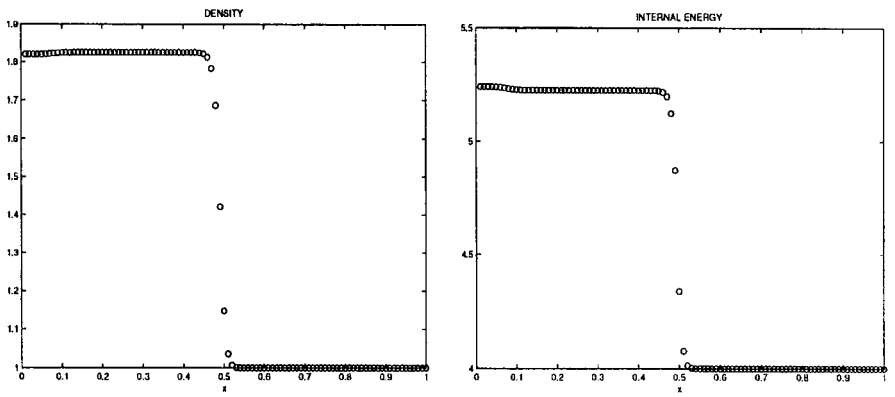

Figure 14. van der Waals EOS. Shock reflection problem with ENO-2 scheme for time $t = 0.4$: density left, internal energy right. All the variables were computed on a equidistant grid of 100 zones.

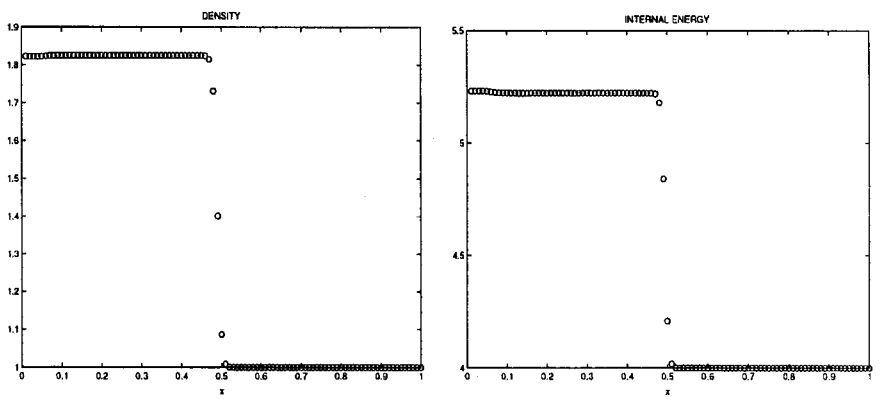

Figure 15. van der Waals EOS. Shock reflection problem with PHM scheme for time $t = 0.4$: density left, internal energy right. All the variables were computed on a equidistant grid of 100 zones.

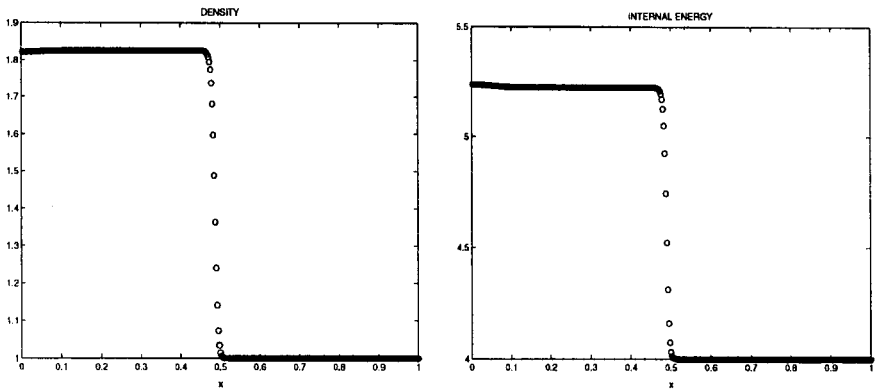

Figure 16. van der Waals EOS. Shock reflection problem with first-order scheme for time $t = 0.4$: density left, internal energy right. All the variables were computed on a equidistant grid of 400 zones.

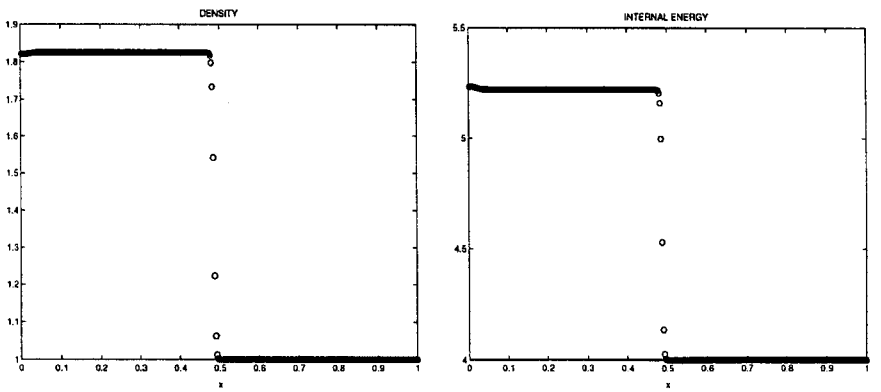

Figure 17. van der Waals EOS. Shock reflection problem with ENO-2 scheme for time $t = 0.4$: density left, internal energy right. All the variables were computed on a equidistant grid of 400 zones.

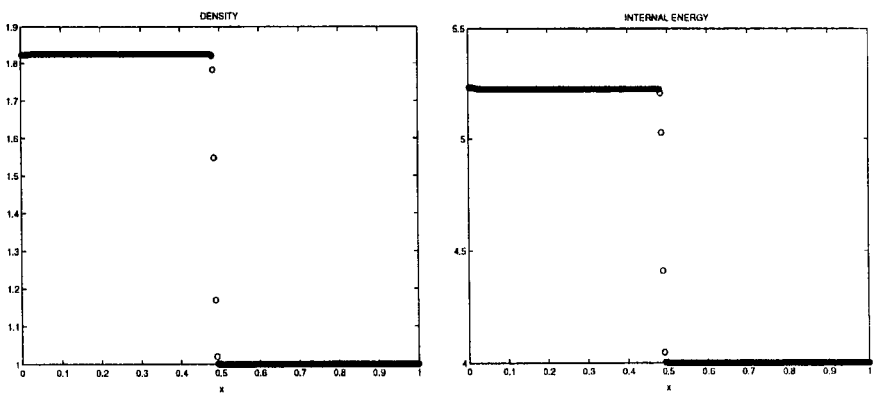

Figure 18. van der Waals EOS. Shock reflection problem with PHM scheme for time $t = 0.4$: density left, internal energy right. All the variables were computed on a equidistant grid of 400 zones.

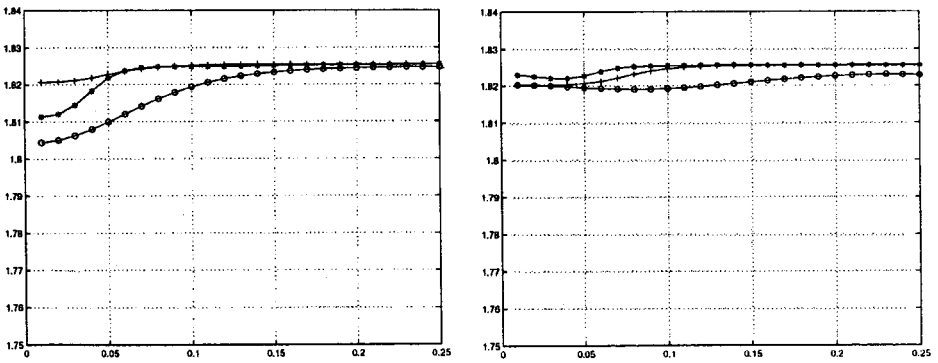

Figure 19. van der Waals EOS, a zoom of 30 grid zone next to the left wall on a 100 zones. Right: present scheme, left: van Leer scheme, o: first-order, +: ENO-2, and *: PHM.

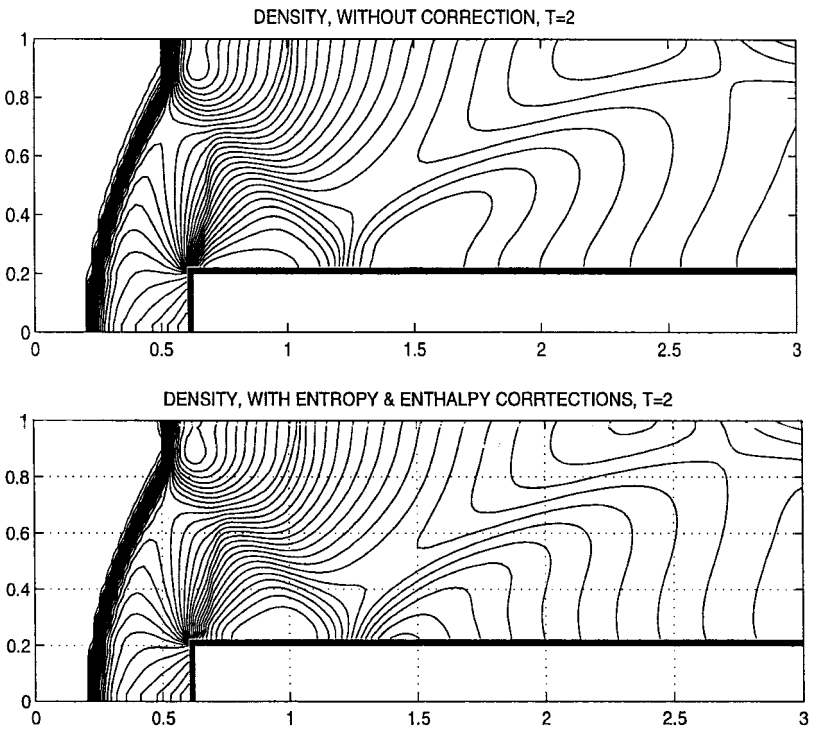

Figure 20. Stiffened gas EOS, contour plots of numerical approximations to the density by the first order scheme: no corner correction (top), with corner correction (bottom) at $T = 2$.

The problem begins with a uniform Mach 3 flow in a wind tunnel containing a step. The tunnel is 3 units long and 1 unit wide. The step is 0.2 units high and is located 0.6 units from the left hand and of the tunnel. An inflow boundary condition is applied at the left end of the computational domain and outflow boundary conditions are applied at the right end.

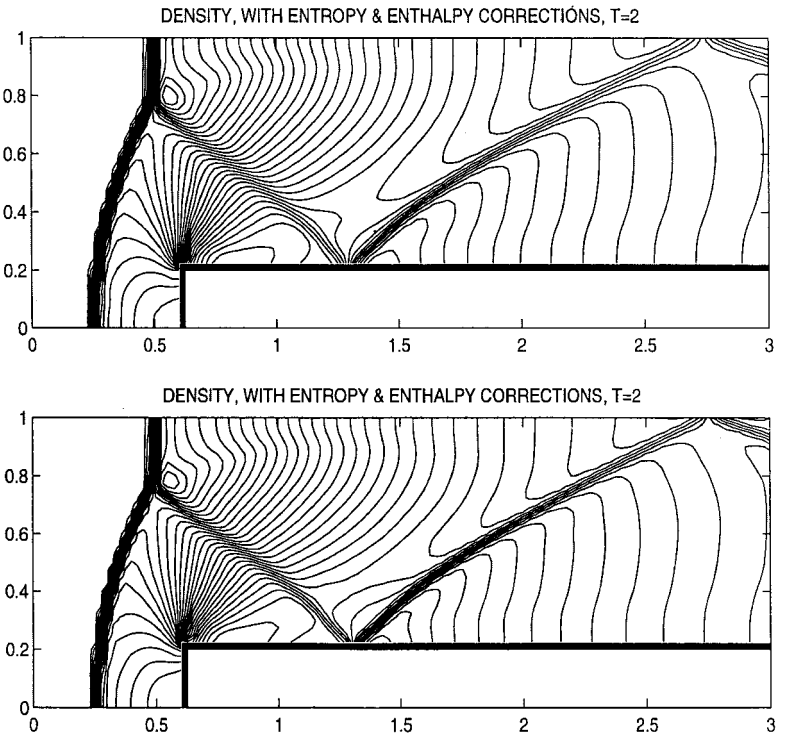

Figure 21. Stiffened gas EOS, contour plots of numerical approximations to the density by ENO-2-REF-M (top), PHM-REF-M (bottom) at $T = 2$. The corner treatment is applied.

We apply reflecting boundary conditions along the walls of the tunnel. The initial conditions for the gas in the tunnel are $\rho = 1.4$, $p = 1$, $u = 3$, and $v = 0$.

The density profile is the hardest to compute due to the numerical errors generated at the corner of the step, which is the centre of the rarefaction fan, i.e. a singular point of the flow, along the upper wall at the contact discontinuity, and along the reflecting boundaries.

Colella and Woodward [16], and Fedkiw *et al.* [15], noticed that these errors generated in the neighbourhood of the corner and along the reflecting boundaries can affect seriously the global flow. A large entropy near the singular point causes a boundary layer in density of about one to two zones to form, and the magnitude of the two components of the velocity decreases along the top of the step. To fix it, it is necessary to apply additional boundary corrections near the corner to minimize the numerical errors: a constant-entropy fix (see Section 4), to enforce entropy constancy, and an enthalpy correction, to get the solution to converge to the steady state.

The corner treatment is performed after updating the computed solution by a substep of the TVD Runge–Kutta methods as follows.

Let us denote by 'a' the cell located just to the left and below the corner, called the reference cell, and by 'b' fours cells of the first row above the step starting just to the right

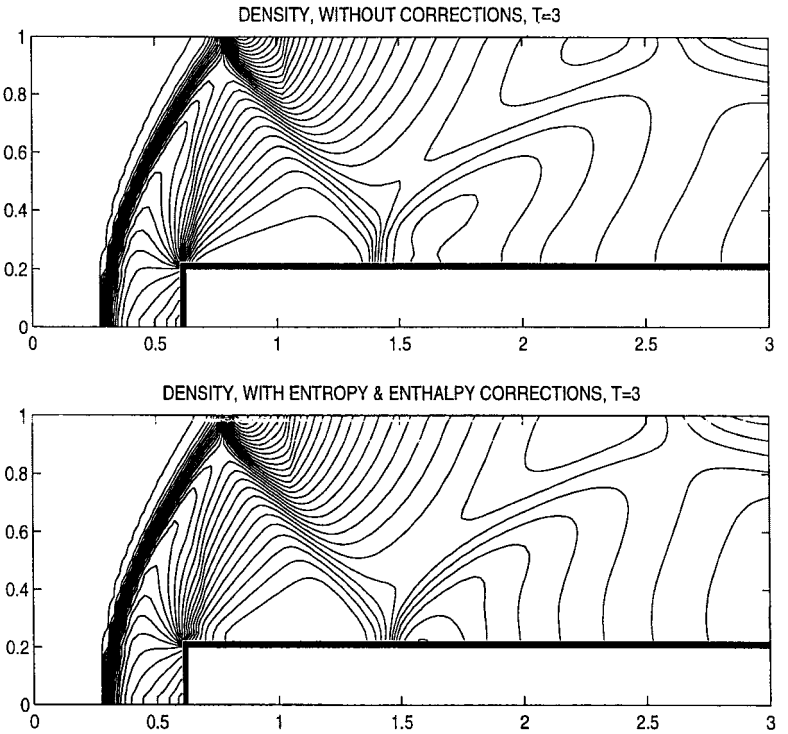

Figure 22. van der Waals EOS, contour plots of numerical approximations to the density by the first-order scheme: no corner correction (top), with corner correction (bottom) at $T = 2$.

of the corner, and the first two cells of the second row above, also starting from the right. We use the conserved variables q_a to correct the variables q_b.

- *Entropy correction*: In each cell 'b' we reset the new density computed in Section 4 from cell 'a' for both Stiffened and van der Waals EOS. Those corrections are consistent since the EOS used have $\Gamma > 0$.
- *Enthalpy correction*: We use the new density value to correct the enthalpy in 'b' cells, by changing the magnitudes of the velocities (not their directions!) as follows:
  There is always a non-negative constant α such that

$$H_a = H_b^{\alpha} \tag{65}$$

  where H_a is the enthalpy in cell 'a', and

$$H_b^{\alpha} = \frac{p_b}{\rho_a} + e_b + \frac{1}{2}\alpha q_b^2 \tag{66}$$

  with $q_b^2 = y_b^2 + v_b^2$. Equation (65) is just Bernoulli's law for steady flows [17], and it always has a non-negative solution for α, because the value of ρ_b is never larger

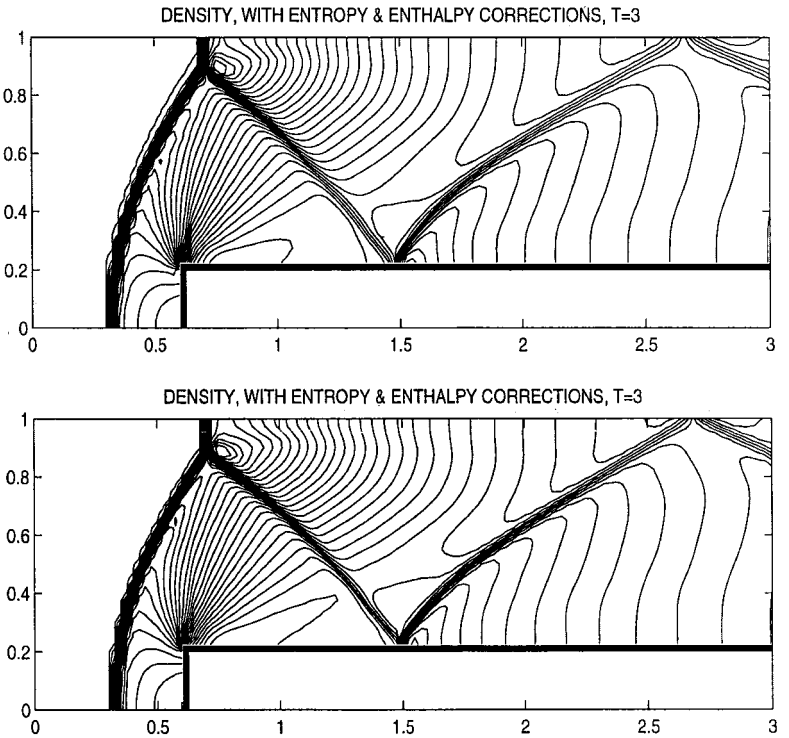

Figure 23. van der Waals EOS, contour plots of numerical approximations to the density: ENO-2-REF-M (top), PHM-REF-M (bottom) at $T = 3$. The corner treatment is applied.

than ρ_a

$$\alpha = \frac{2(H_a - p_b/\rho_b - e_b)}{q_b^2} \tag{67}$$

The new conserved variables are

$$\mathbf{q}_b = (\rho_{\text{new}}, \sqrt{\alpha}\rho_{\text{new}} u_b,\ \sqrt{\alpha}\rho_{\text{new}} v_b,\ \rho_{\text{new}} e_b + \rho_{\text{new}}\alpha(u_a^2 + v_a^2/2))^{\mathrm{T}} \tag{68}$$

Such corner correction is accompanied by an entropy correction along the upper wall of the tunnel to reduce overheating errors.

We run the code, with equally spaced grids $\Delta x = \Delta y = \frac{1}{40}$, and display the numerical results when the unsteady flow has a rich and interesting structure. Each plot (Figures 20–23) displays 30 equally spaced level curves between the minimum and maximum values of the computed density.

Figures 24–26 show the effect of the numerical corner treatment and isobaric fix. The overheating errors are reduced (the level curves near the wall are more orthogonal). Observe that the Mach stem pathology at the contact discontinuity is minimized and the entropy at the corner is preserved. Also, we see that the Mach stem and the position of the reflected

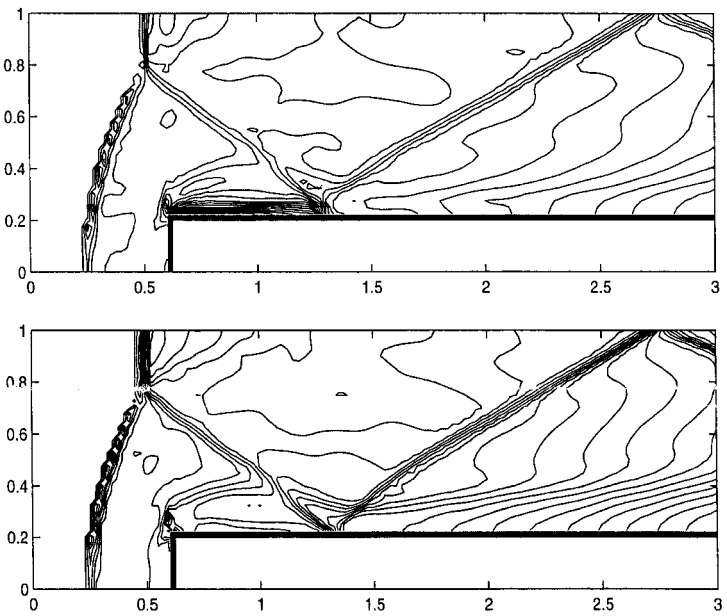

Figure 24. Stiffened EOS, contour plots of numerical approximations to the enthalpy by the PHM scheme: no corner correction (top), with corner correction (bottom) at $T = 3$. Notice the entropy violation near the corner and the build up of the boundary layer.

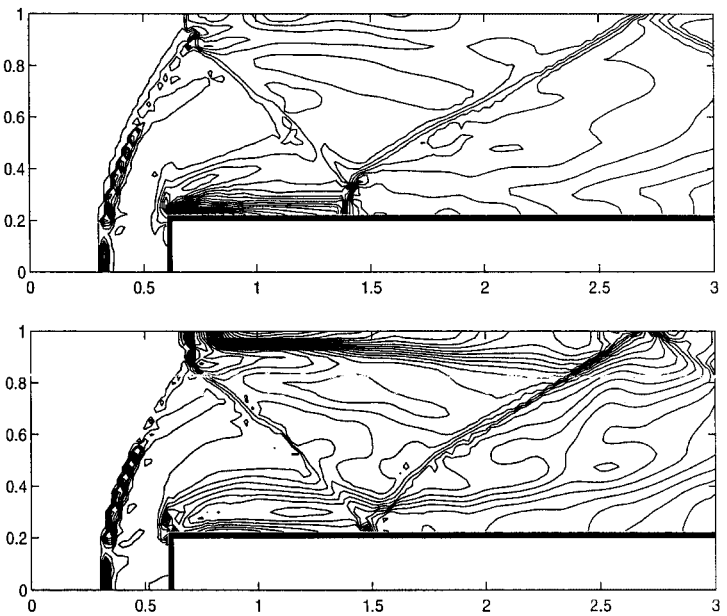

Figure 25. van der Waals EOS, contour plots of numerical approximations to the enthalpy by the PHM scheme: no corner correction (top), with corner correction (bottom) at $T = 3$. Notice the entropy violation near the corner and the build up of the boundary layer.

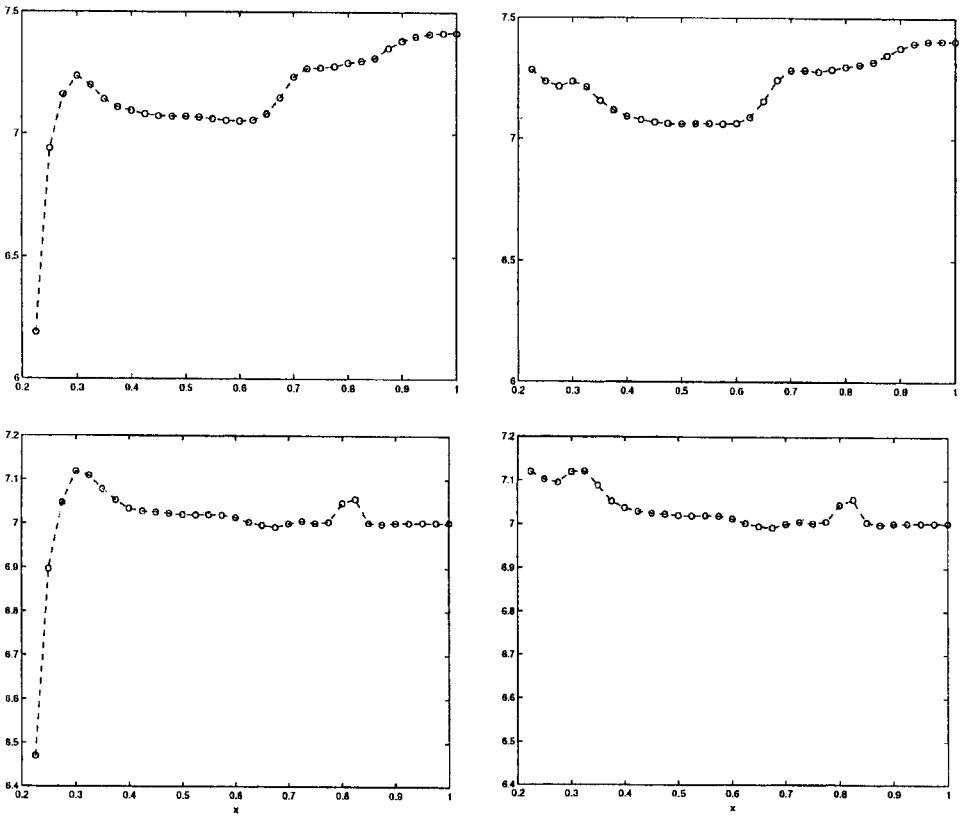

Figure 26. Section $x = 0.605$ of the enthalpy. Top: Stiffened EOS. Bottom: van der Waals EOS. Left: no corner treatment. Right: with corner treatment.

shock are consistent in all runs. The order of accuracy of the method used is consistent with resolution obtained.

6. CONCLUSION

An extension of the flux split method [2] to an arbitrary equilibrium gas law has been described. The scheme is non-linear, uniquely defined, upwind, and introduces numerical dissipation in a natural way. The evaluation of the flux function uses directly the point values of the thermodynamical derivatives without any assumption or approximation.

An extension of Bernoulli's law, to get the solution to converge to steady state, and an entropy correction for both Stiffened gas and van der Waals EOS, to reduce the overheating near material interfaces, has also been introduced.

From the numerical results, it is clear that the present scheme is as robust and efficient as in the perfect gas case.

REFERENCES

1. Noh W. Errors for calculations of strong shocks using an artificial heat flux. *Journal of Computational Physics* 1987; **72**:78–120.
2. Donat R, Marquina A. Capturing shock reflections: an improved flux formula. *Journal of Computational Physics* 1996; **125**:42–58.
3. Quirk JJ. A contribution to the great Riemann solver debate. *International Journal for Numerical Methods in Fluids* 1994; **18**:555–574.
4. Abgrall A. An extension of Roe's upwind scheme to algebraic equilibrium real gas models. *Computers and Fluids* 1991; **19**:171–182.
5. Colella P, Glaz HM. Efficient solution algorithms for the Riemann problem for real gases. *Journal of Computational Physics* 1985; **59**:264–289.
6. Glaister P. An approximate linearized Riemann solver for the Euler equations for real gases. *Journal of Computational Physics* 1988; **74**:382–408.
7. Glaister P. An approximate linearized Riemann solver for the three-dimensional Euler equations for real gases using operator splitting. *Journal of Computational Physics* 1988; **77**:361–383.
8. Muller E. Flux vector splitting for the Euler equations for real gases. *Journal of Computational Physics* 1988; **79**:227–230.
9. Liu MS, van-Leer B, Shuen JS. Splitting of inviscid fluxes for real gases. *Journal of Computational Physics* 1990; **87**:1–24.
10. Menikoff R, Plohr BJ. The Riemann problem for fluid flow of real material. *Review of Modern Physics* 1989; **61**:75–130.
11. Atkins P. *Physical Chemistry* (5th ed). Freeman: New York, 1994.
12. Shu CW, Osher S. Efficient implementation of essentially non-oscillatory shock capturing schemes (two). *Journal of Computational Physics* 1989; **83**:32–78.
13. Stiriba Y. A nonlinear flux split method for hyperbolic conservation laws. *Journal of Computational Physics* 2002; **176**:20–39.
14. Marquina A. Local piecewise hyperbolic reconstruction of numerical fluxes for nonlinear scalar conservation laws. *SIAM Journal of Science and Computing* 1994; **15**:892.
15. Fedkiw R, Marquina A, Merriman B. An isobaric fix for the over-heating problem in multimaterial compressible flows. *Journal of Computational Physics* 1999; **148**:545–578.
16. Woodward P, Colella P. The numerical simulation of two-dimentional fluid flow with strong shock. *Journal of Computational Physics* 1984; **54**:115–173.
17. Courant R, Friedrichs KO. Supersonic flow and shock waves. *Applied Mathematical Sciences*, vol. 21. Springer: New York, 1976.
18. Fedkiw R, Merriman B, Donat R, Osher S. The penultimate scheme for systems of conservation laws: finite difference ENO with Marquina's flux splitting. *UCLA CAM Report*, July 1996; 96–18.

